

UNCLASSIFIED

AD 268 135

*Reproduced
by the*

**ARMED SERVICES TECHNICAL INFORMATION AGENCY
ARLINGTON HALL STATION
ARLINGTON 12, VIRGINIA**



UNCLASSIFIED

NOTICE: When government or other drawings, specifications or other data are used for any purpose other than in connection with a definitely related government procurement operation, the U. S. Government thereby incurs no responsibility, nor any obligation whatsoever; and the fact that the Government may have formulated, furnished, or in any way supplied the said drawings, specifications, or other data is not to be regarded by implication or otherwise as in any manner licensing the holder or any other person or corporation, or conveying any rights or permission to manufacture, use or sell any patented invention that may in any way be related thereto.



TECHNICAL NOTE

D-701

PHYSICAL SIGNIFICANCE OF THE TIROS II RADIATION EXPERIMENT

R. A. Hanel
Goddard Space Flight Center

and

D. Q. Wark
U. S. Weather Bureau

NATIONAL AERONAUTICS AND SPACE ADMINISTRATION
WASHINGTON

December 1961

NASA TN D-701

ASTIA

268135

NOX
62-1-5

PHYSICAL SIGNIFICANCE OF THE TIROS II RADIATION EXPERIMENT

by

R. A. Hanel

Goddard Space Flight Center

and

D. Q. Wark

U. S. Weather Bureau

SUMMARY

The meteorological satellite TIROS II carries a five-channel radiometer which scans the earth as the satellite rotates. Two channels are sensitive to sunlight reflected from the earth; three are responsive to terrestrial infrared emission. The effect of the optical properties upon the measurements is discussed. Calculations based on model atmospheres show the sources of outgoing terrestrial radiation and limb-darkening effects for two of the channels. A map of the radiation received by the channel sensitive in the window region (8 to 12 μ) is compared with a conventional weather chart.

CONTENTS

Summary	i
INTRODUCTION	1
THE MEDIUM RESOLUTION RADIOMETER	1
TERRESTRIAL INFRARED RADIATION	8
TIROS II MEASUREMENTS	11
CONCLUSION	15
ACKNOWLEDGMENTS	15
References	15

PHYSICAL SIGNIFICANCE OF THE TIROS II RADIATION EXPERIMENT*

by

R. A. Hanel

Goddard Space Flight Center

and

D. Q. Wark

U. S. Weather Bureau

INTRODUCTION

The meteorological satellite TIROS II, launched into orbit in November 1960, carries two television cameras and two infrared radiometers. The low resolution radiometer performs a heat balance measurement. By sensing the temperatures of a black and a white detector, the experiment discriminates between terrestrial thermal radiation and reflected sunlight. Both detectors are thermally isolated from the satellite and exposed to the same area on earth as the wide angle television camera (Reference 1).

This paper discusses the physical significance of measurements by the five-channel medium resolution radiometer (cf. Reference 2). The systems aspect of this experiment and the instrumental details of the radiometer have been described elsewhere (References 3 and 4).

THE MEDIUM RESOLUTION RADIOMETER

The optical axis of the radiometer revolves around the spin axis of the satellite in a double cone which has a half-angle of 45 degrees. The scan pattern on the earth varies from a circle, when the spin axis points towards the center of the earth, to two alternating

*This paper was presented at the March, 1961 meeting of the Optical Society of America in Pittsburgh, Pennsylvania.

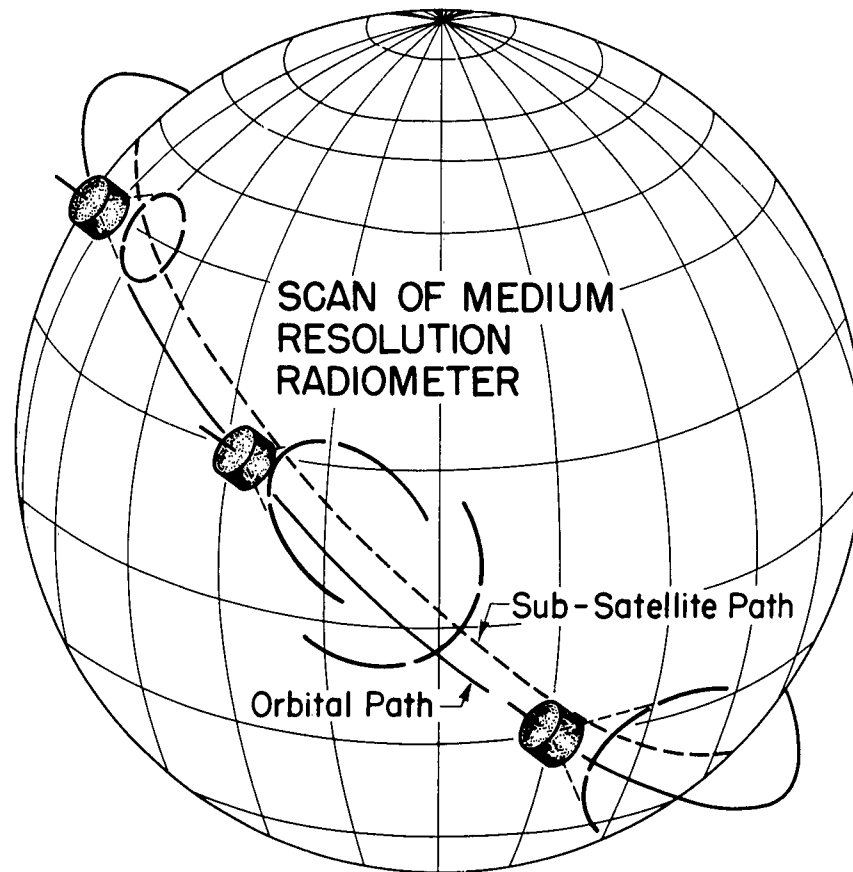


Figure 1—The scan patterns of the Tiros II medium resolution radiometers, viewed at 45 degrees from the spin axis

hyperbola-like branches, about a quarter of an orbit later, when the spin axis is tangential to the earth (Figure 1). The 45-degree scan geometry was chosen because it gives maximum coverage from a spin-stabilized satellite. The radiometer is mounted in the satellite so that the view in one direction is through a hole in the floor, or base plate, and in the other direction through a hole in the side wall. These openings can be seen in Figure 2, which is a bottom view of the entire satellite.

The medium resolution radiometer is a cluster of five almost identical elements, each responsive to a different region of the electromagnetic spectrum. The principle of operation of one channel is shown in Figure 3. The alternating voltage generated at the thermistor bolometer is proportional to the difference between the energy absorbed by the bolometer when the chopper disk is in the position shown in Figure 3 and when it is in the diametrically opposite position. In the figure, w is the radiant emittance of the viewed source, R the reflectivity, ϵ the emissivity, and f the transmission of the lens-filter combination. Superscripts f and w refer to the floor and wall directions; and m and b ,

TN D-701



Figure 2—Bottom view of the Tiros II satellite. Viewing ports for the five-channel medium resolution radiometer are in the side (top of figure), and in the base adjacent to the mounting ring.

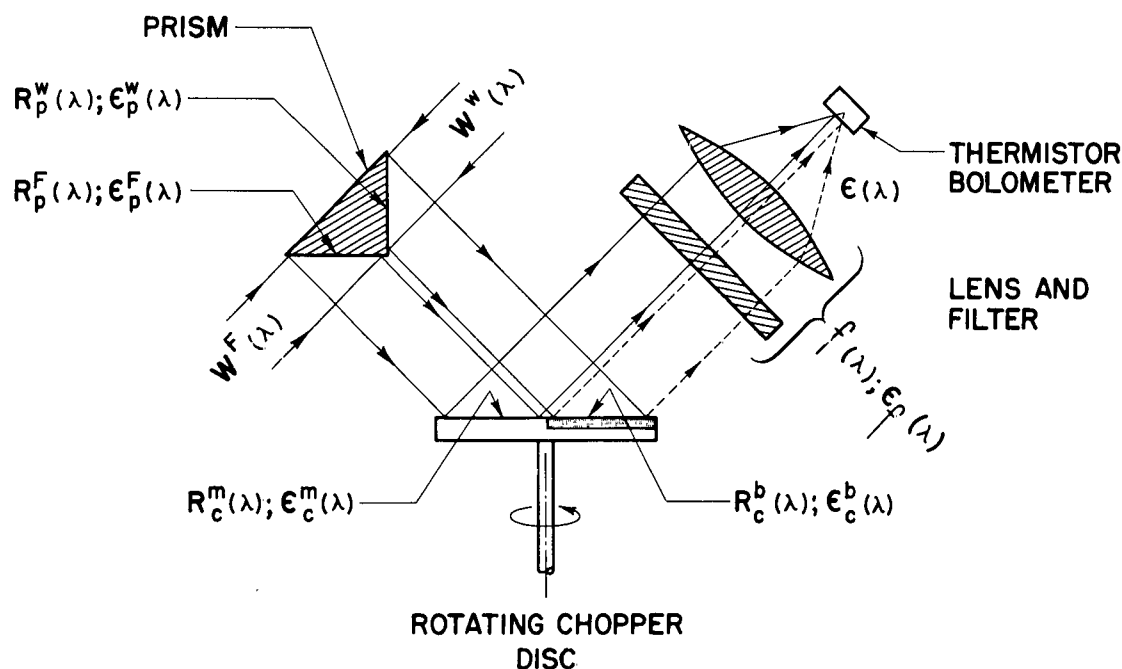


Figure 3—Optical configuration of one channel of a Tiros II medium resolution radiometer. Radiation from opposite directions is reflected by the prism-shaped mirror onto the chopper, thence through the filter and lens to the bolometer.

refer to the mirror and black sides of the chopper disc. Subscript p indicates the prism, and c the chopper.

The bolometer absorbs radiation originating within the field of view on the wall side $W^W(\lambda)$ and the floor side $W^F(\lambda)$ of the radiometer. The intensity and spectral distribution of the received radiation is modified by the reflecting surfaces of the prism and of the chopper, but mainly by the transmission characteristic of the filters and lenses. Each optical element in the system contributes to the radiation incident on the detector according to its own emissivity and temperature. In a properly balanced and aligned instrument, the energy difference is

$$\Delta W = \int_0^\infty \epsilon \left[\left(W^W R_p^W R_c^b f + \epsilon_p^W W_p^W R_c^b f + \epsilon_c^b W_c^b f + \epsilon_f W_f + W^F R_p^F R_c^m f + \epsilon_p^F W_p^F R_c^m f + \epsilon_c^m W_c^m f + \epsilon_f W_f \right) \right. \\ \left. - \left(W^W R_p^W R_c^m f + \epsilon_p^W W_p^W R_c^m f + \epsilon_c^m W_c^m f + \epsilon_f W_f + W^F R_p^F R_c^b f + \epsilon_p^F W_p^F R_c^b f + \epsilon_c^b W_c^b f + \epsilon_f W_f \right) \right] d\lambda. \quad (1)$$

Since some terms in Equation 1 compensate each other and if optical properties and temperatures on both sides of the prism are assumed to be equal, then ΔW becomes

$$\Delta W = \int_0^{\infty} \left[W_{(\lambda)}^W - W_{(\lambda)}^F \right] \phi(\lambda) d\lambda, \quad (2)$$

where $\phi(\lambda)$ characterizes the effective spectral response

$$\phi(\lambda) = R_p \left(R_c^b - R_c^m \right) f \epsilon. \quad (3)$$

The nominal wavelength limits of the five channels are

- (1) 6 to 6.5 Microns - water vapor absorption
- (2) 8 to 12 Microns - atmospheric window
- (3) 0.2 to 6 Microns - reflected solar radiation
- (4) 8 to 30 Microns - terrestrial radiation
- (5) 0.55 to 0.75 Microns - vidicon response

The effective spectral responses, $f \left(1 - R_c^b / R_c^m \right)$, of the infrared channels (1, 2, and 4), are plotted against wave number in cm^{-1} in the upper part of Figure 4; the nonlinear wavelength scale is also shown. Reflection of all aluminized optical surfaces and the emissivity of the thermistor bolometer are considered to be independent of wavelength, although this may not be fully justified at all wavelengths. The lower portion of Figure 4 shows the specific spectral intensity of a blackbody at 300°K and the principal absorption bands of the atmosphere. The amount of radiation detectable by the satellite depends upon the temperature structure of the atmosphere in view; the vertical distribution of the absorbing gases; and the height, amount, and density of clouds.

The spectral region of channel 1 is centered in the 6.3 micron water vapor band. The second channel observes radiation in the 8 to 12 micron "window." This window is not totally transparent; the influence of the ozone band at 9.6 microns and weak absorption due mainly to water vapor have to be considered. Channel 4 (8 to 30 microns) covers the window as well as portions of the spectrum wherein water vapor and carbon dioxide possess strong absorption bands.

The effective filter functions of channels 3 and 5, which are sensitive to reflected solar radiation, are shown in the upper part of Figure 5. The lower portion depicts: solar radiation reaching the surface, with several atmospheric absorption bands indicated as dark areas; Rayleigh scattering, in relative terms only; and a response curve of the vidicon tubes used in the TIROS II television cameras. The response of channel 5 coincides approximately with the spectral sensitivity of the vidicons. Channel 3 is nearly flat over the solar spectrum.

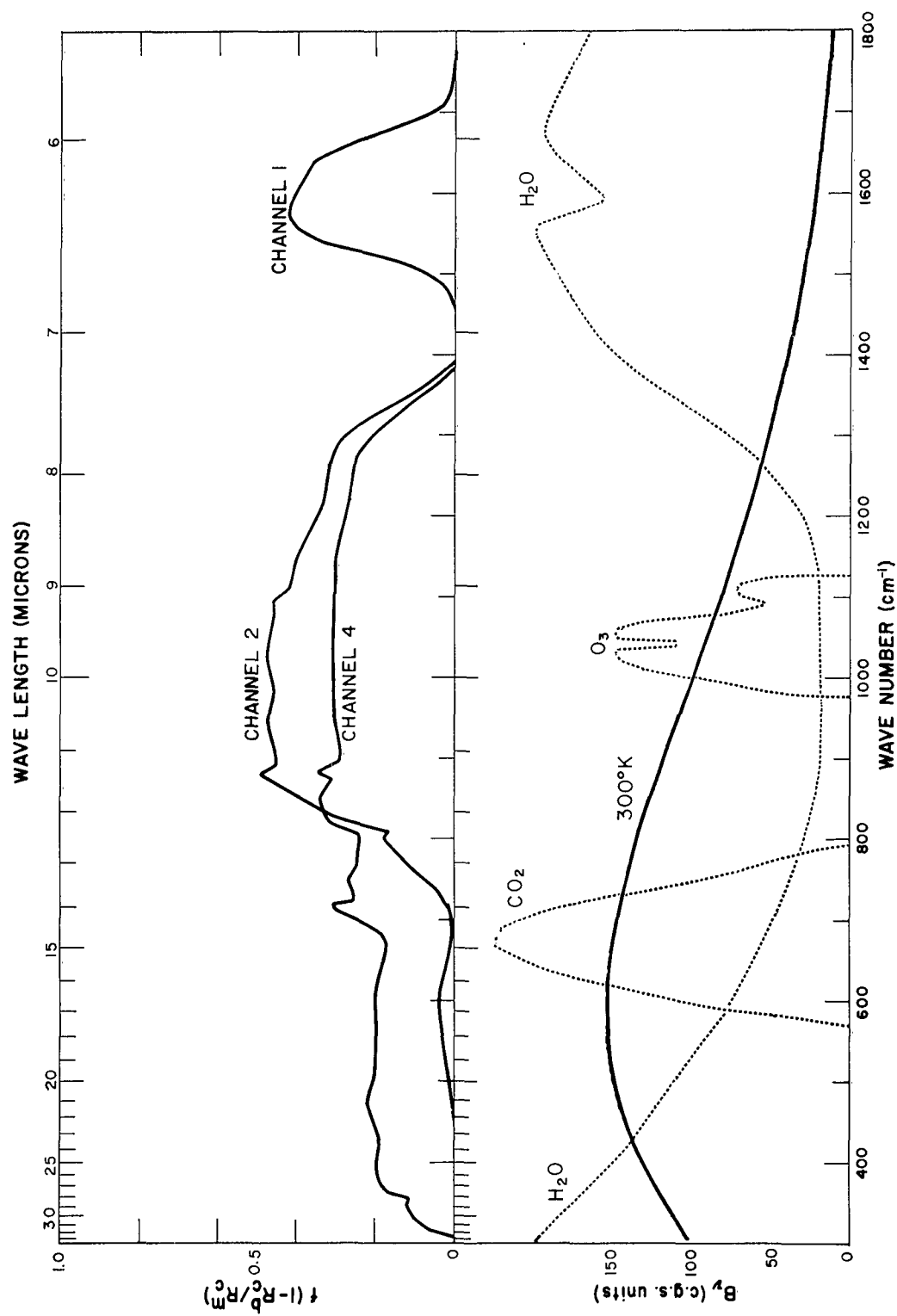


Figure 4—The terrestrial channels. The upper portion shows the effective filter functions for channels 1, 2, and 4. Filter, lens, and chopper reflectivity characteristics are included. The lower portion pictures the principal absorption bands of the atmosphere (qualitatively) and blackbody specific intensity for 300°K.

D-701

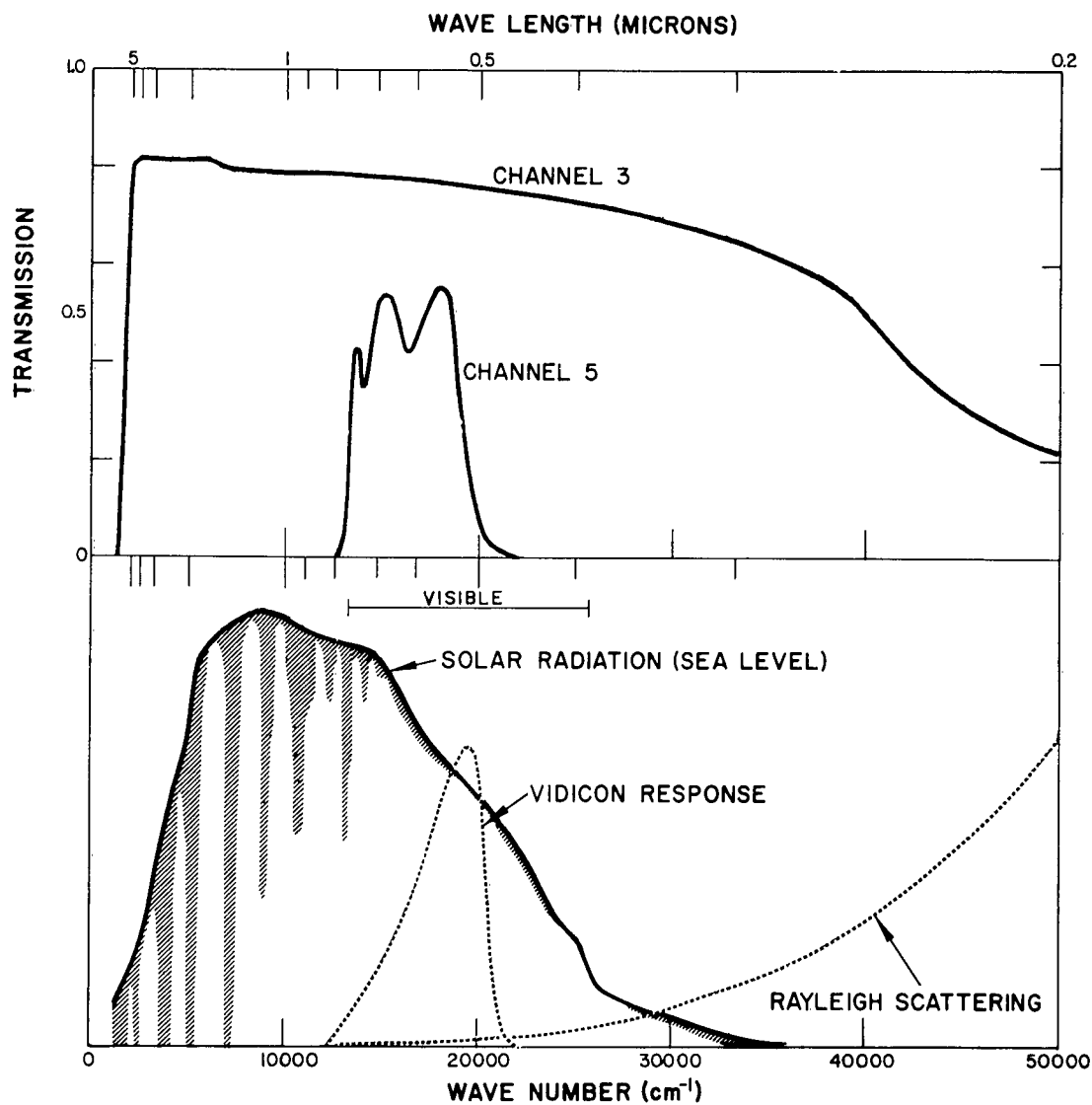


Figure 5—The reflected solar radiation channels. The effective filter functions for channels 3 and 5 are shown in the upper portion. Below are graphed: the solar radiation received at the surface, with the atmospheric absorption bands shaded; the average response of the Tiros vidicons; and the relative effect of Rayleigh scattering.

TERRESTRIAL INFRARED RADIATION

For a meaningful interpretation of data, it is not enough merely to consider the spectral sensitivity of the instrument. The contribution of all atmospheric levels to the total amount of radiation received by the satellite must be studied. Typical atmospheric models, as constructed from radiosonde data, give temperature and composition as a function of pressure. The intensity of radiation emerging from a stratified atmosphere was calculated in narrow spectral bands for several zenith angles. Methods of calculation and the application of the results are discussed elsewhere (References 5, 6, 7, 8).

The temperature and the water vapor mixing ratio of a model atmosphere are plotted in the left part of Figure 6. The temperature scale is linear here and the other scales are logarithmic. Height is also nearly linear, with the surface at the bottom and a height of about 50 kilometers corresponding to the top of the figure. On the right are shown the fractional contributions dI/I to the intensity of outgoing radiation in the vertical direction, as a function of pressure, for channels 1 and 2. Channel 4 (8 to 30 microns) would lie somewhere between the two curves. Both curves have been normalized to the total effective upward radiation represented by the unit area delineated by the dashed line. These curves are derived from the formula

$$\frac{dI}{I} = \frac{\int_0^{\infty} \phi(\lambda) B(\lambda, T) d[\tau(\lambda)] d\lambda}{\int_0^{\infty} \int_0^1 \phi(\lambda) B(\lambda, T) d[\tau(\lambda)] d\lambda}, \quad (4)$$

in which $\tau(\lambda)$ is the transmission from a given level to the top of the atmosphere and $B(\lambda, T)$ is the Planck intensity.

Radiation measured by channel 1 originated almost entirely in the atmosphere. In this particular model it came from a layer centered at about 400 mb. Approximately 0.4 mm of precipitable water lies above this level. Radiation registered by channel 2 came mostly from the ground, and from cloud tops if they were present; about 25 percent originated in the lower part of the atmosphere. The atmospheric contribution to the channel 2 signals must be taken into account in the interpretation of data, especially in moist air and at large zenith angles. Ozone was not included in this calculation, but it must be in any refined interpretation. Channel 4, if included, would show about half of the radiation coming from the atmosphere.

As the satellite spins and progresses along its path, the radiometers view the earth at constantly changing angles. The measurement depends not only upon the nature of the atmosphere but also upon the angle of view. The outward radiation is a function of the optical path and the temperature distribution in the atmosphere. Where temperature decreases with height, limb darkening occurs and data should be corrected for it. Because

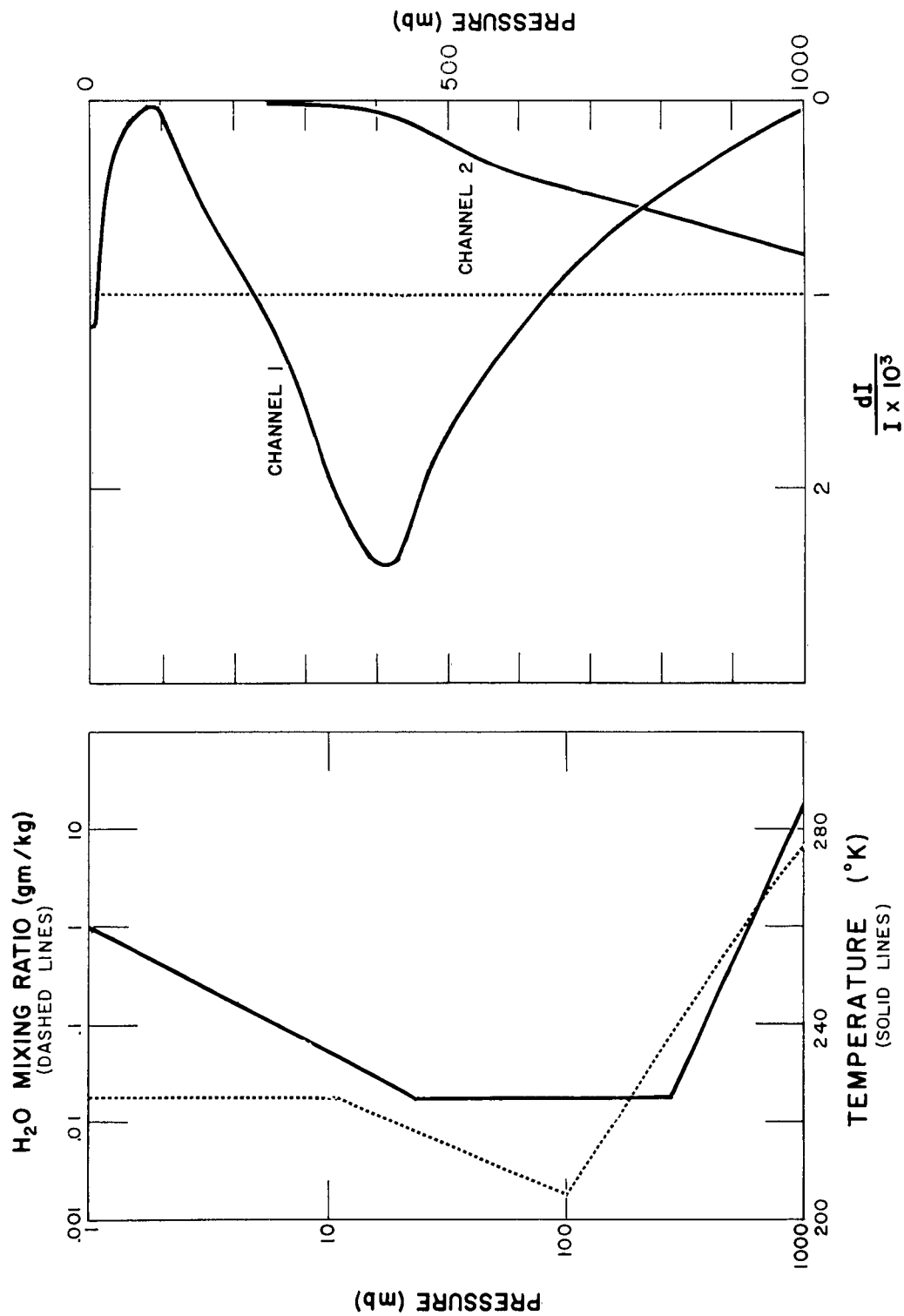


Figure 6—Upward radiation. On the left is a model atmosphere: the solid line is temperature versus pressure, and the dashed line is water vapor mixing ratio versus pressure. On the right are the normalized contributions to the upward radiation for channels 1 and 2. The dashed line encloses unit area; the dimension of its abscissa is mb^{-1} .

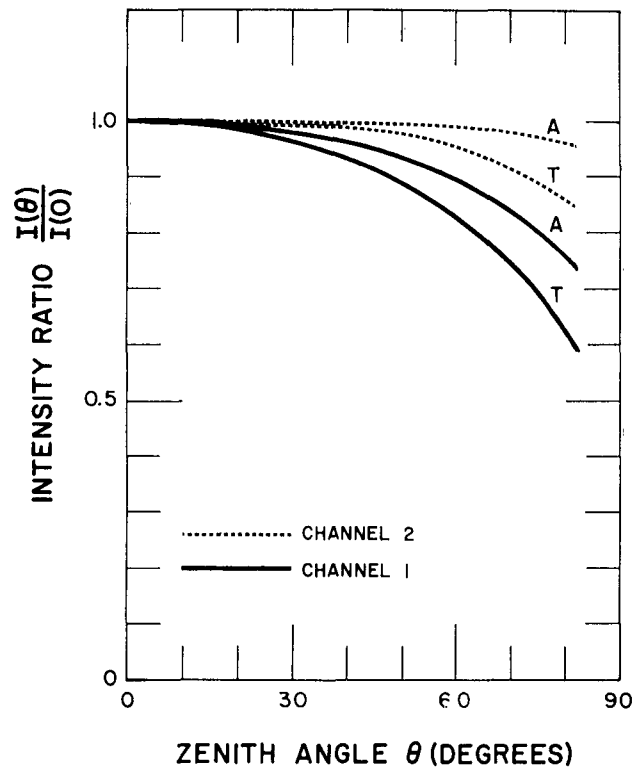


Figure 7—Limb darkening for channels 1 and 2. The ratio of the intensity at zenith angle θ to the intensity in the vertical is drawn versus θ . T indicates a tropical atmosphere, A an Arctic atmosphere.

of the variations in composition and temperature of the atmosphere over even relatively short distances, there is no general law of limb darkening. But by using model atmospheres, the normal range to be expected in limb darkening as a function of the local zenith angle can be calculated (Figure 7). The ordinate is the ratio of outgoing intensity (as defined by the denominator in Equation 4), in a particular direction, to the radiation in the vertical; and the abscissa is the zenith angle, θ . The two dashed lines represent channel 2, the window, as it might view tropical (T) and arctic (A) regions. Because the Arctic is drier and usually possesses a smaller temperature gradient with height, the effect is smaller there. The two solid lines represent channel 1, the water vapor band, also for tropical and arctic regions. Here, too, the effect in the Arctic is less; but because the radiation comes almost entirely from the atmosphere, the effect is much greater than for either region in channel 2. In a first approximation the effect might be ignored for channel 2 except at very large angles; but it must be taken into account for channel 1, except at very small angles.

TIROS II MEASUREMENTS

Three consecutive sweeps of channel 2 are shown as typical scan patterns in Figure 8. The signal between the sweeps corresponds to the zero radiation level, i.e., when the radiometer was viewing space; and the ordinate is approximately proportional to the energy received by the detector.

Figure 9 is a surface weather chart for 1200 GMT, November 25, 1960. The dashed line is the sub-satellite path about 45 minutes after the observation time of this chart. Clearly visible are two prominent low pressure centers, with associated frontal systems. The system on the left is young and vigorous, whereas the larger one to the northeast is older and the frontal system there is progressing out of the low. There is generally high pressure along the lower portion of the chart.

The radiation map made from measurements by channel 2 is shown in Figure 10. Isotherms of equivalent blackbody radiation are shown in °C. The fronts which appeared on the weather chart also are on this figure. The relative accuracy of the temperature measurement is $\pm 2^{\circ}\text{C}$. Absolute values may vary by as much as $\pm 5^{\circ}\text{C}$ when second order effects in the calibration procedure are taken into account. The values in Figure 10 should not be interpreted as temperatures of viewed objects; they are the temperatures of a blackbody which would give the same output from the radiometer as the measured quantities. In some cases, such as in the views of the tops of very dense undercast clouds or of the surface where no clouds are present and the air is dry, the values should be near actual temperatures.

The swaths of data, if they were shown, would be arcs crossing the path of the satellite. There were about 90 swaths, containing about 3000 points, in the area covered by the contours.

In advance of the front on the left of the picture is a region of marked low temperatures, indicating an area of cloud tops which are high and therefore cold; this is to be expected from the classical cloud structure associated with storms of this type. Immediately behind the front, the sharply rising temperatures indicate rapidly clearing skies, at least of the higher cloud types.

The second frontal system does not show the same feature; instead, it lies through a region of high temperature off the coast of the Iberian peninsula. This indicates a very weak and dissipating front. It no longer has much cloudiness associated with it; the radiation comes from the ocean or from the tops of low, and therefore warmer, clouds. Farther south, however, there appears to be some activity still associated with this front, indicated by the lower temperatures.

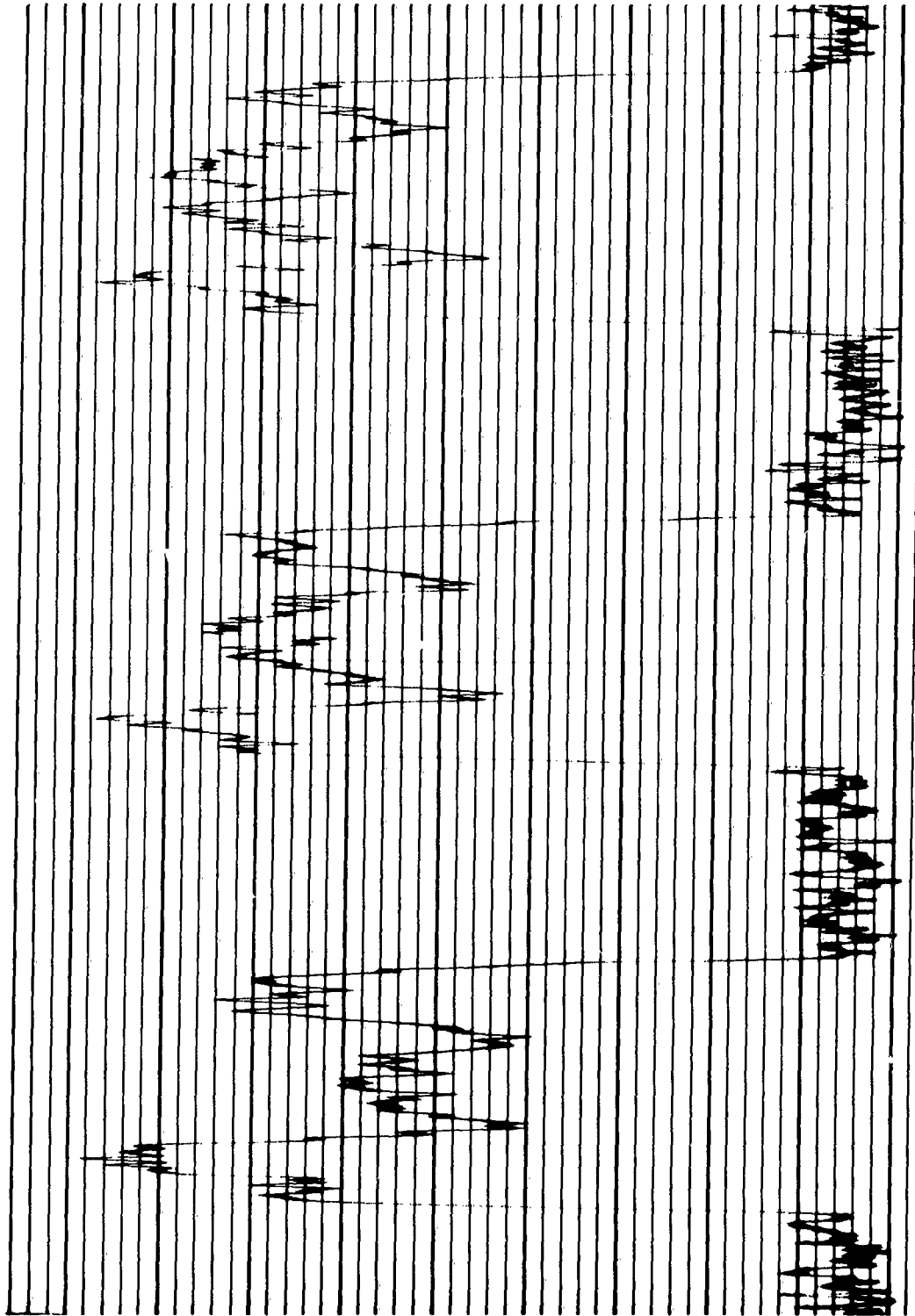


Figure 8 - Scan patterns for three sweeps of channel 2. The ordinate is proportional to the energy received by the detector. Between the sweeps the radiometer was viewing space.

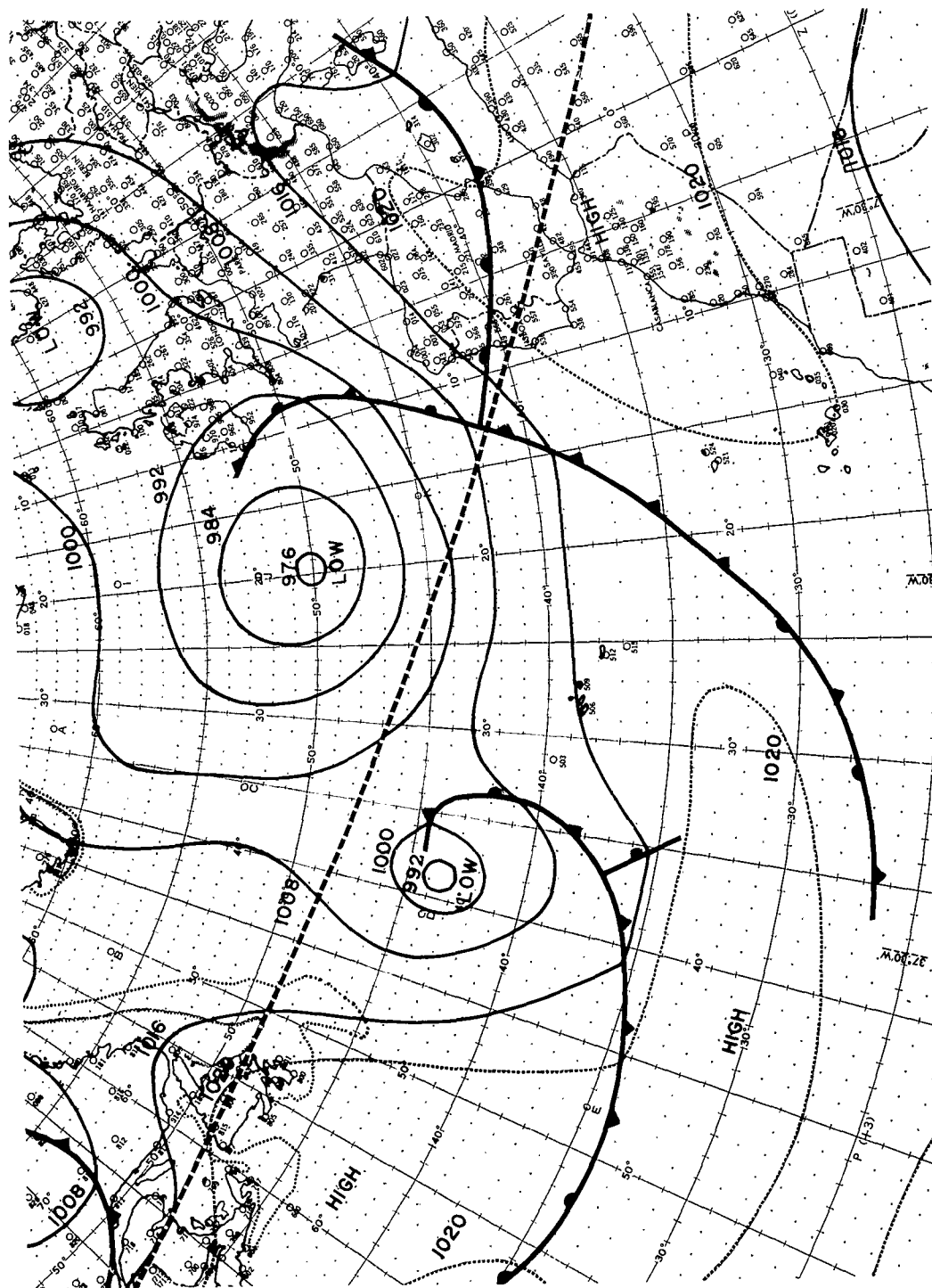


Figure 9—Surface weather chart over the Atlantic Ocean for 1200 GMT, November 25, 1960.
The dashed line is the sub-satellite path.

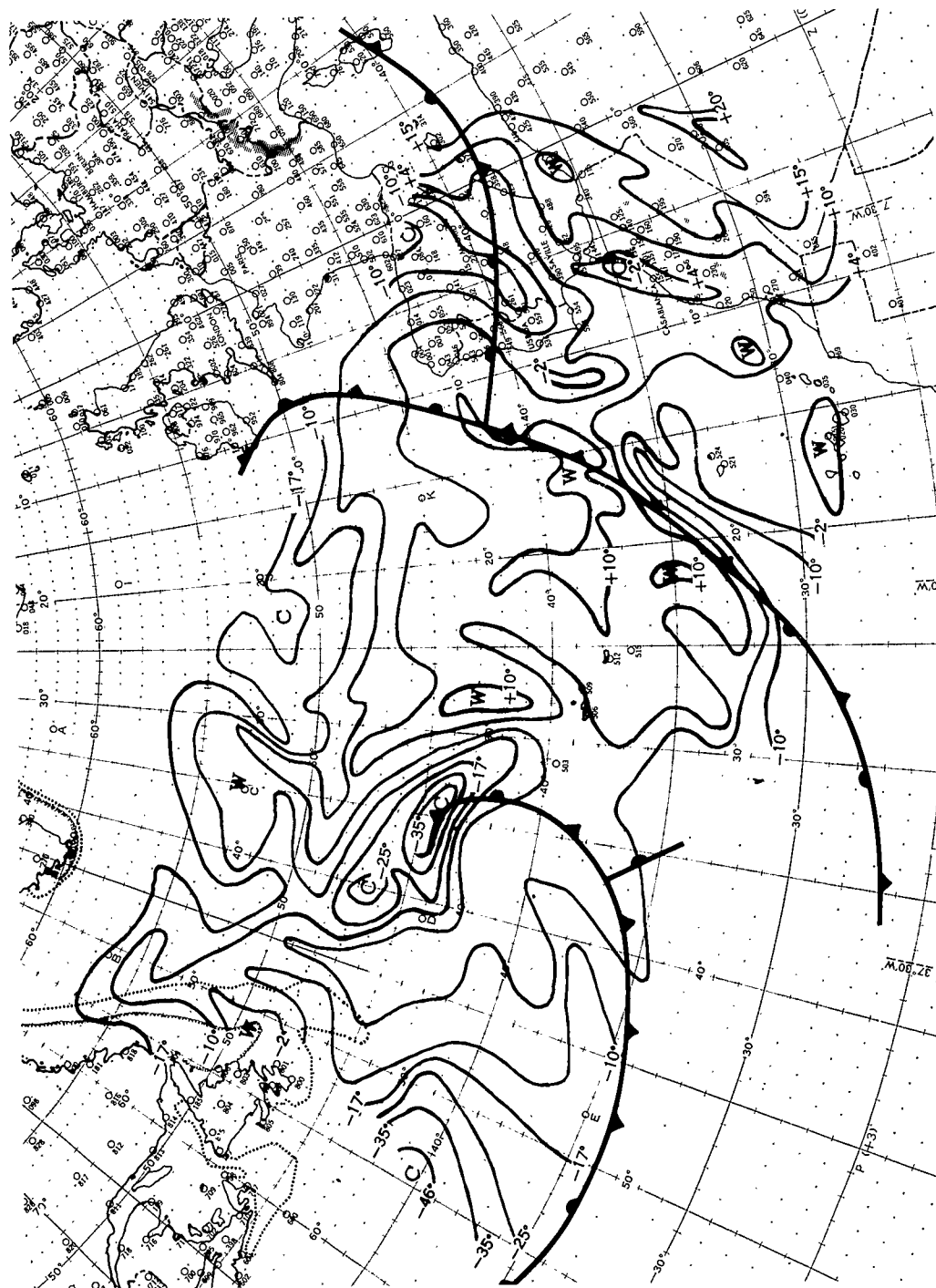


Figure 10—Tiros II radiation map for channel 2 (8 to $12\ \mu$), pass 30, 1245 GMT, November 25, 1960. The isotherms are equivalent blackbody temperatures in $^{\circ}\text{C}$. The weather fronts from Figure 9 are included in this figure.

The lowest values of temperature are on the far left. Just off the chart is a newly developed low center; the low temperatures probably indicate a shield of high, thick clouds extending well in advance of this new system.

Several other interesting features may be distinguished. The trough of low values over the Iberian peninsula is probably related to an older front which is not indicated on the weather chart but which still retains its clouds. Low values are centered near 52°N; 23°W and 47°N; 40°W. These might be near the centers of the upper-air lows connected with the surface lows. A small low area along the Moroccan coast suggests a patch of coastal cloudiness.

CONCLUSION

First results of the TIROS II medium resolution radiation experiment indicate the intimate relation between the weather and upward radiation. Features not adequately revealed by conventional surface weather charts show clearly in maps constructed from TIROS II data.

ACKNOWLEDGMENTS

There were too many contributors to this experiment to permit an expression of gratitude to each. The authors would like, however, to thank R. T. Hite of the U. S. Weather Bureau and W. R. Bandeen of the Goddard Space Flight Center for work which led to the final output of the data presented in this paper.

REFERENCES

1. Hanel, R. A., "Low Resolution Unchopped Radiometer for Satellites," ARS J. 31(2):246-250, February 1961; also NASA Technical Note D-485, February 1961
2. Hanel, R. A., and Stroud, W. G., "Infrared Imaging from Satellites," J. of SMPTE 69(1):25-26, January 1960
3. Bandeen, W. R., Hanel, R. A., et al., "Infrared and Reflected Solar Radiation Measurements from the TIROS II Meteorological Satellite," presented at AMS meeting, New York, January 1961; NASA Technical Note D-1096, 1961
4. Astheimer, P. W., DeWaard, D., and Jackson, E. A., paper presented at the OSA meeting, Pittsburgh, Pa., March 3, 1961

5. Elsasser, W. M., and Culbertson, M. F., "Atmospheric Radiation Tables," American Meteorol. Soc., Meteorol. Monographs, Vol. 4, No. 23, August 1960
6. Wark, D. Q., "On Indirect Temperature Soundings of the Stratosphere from Satellites," J. Geophys. Res. 66(1):77-82, January 1961
7. Wark, D. Q., private communication; paper in preparation
8. Wark, D. Q., and Yamamoto, G., "Methods of Transforming Terrestrial Infrared Radiation Measurements Made from Satellites," paper presented at 41st Annual Meeting of the AMS, New York, January 1961, to be published

TN D-701

<p>NASA TN D-701 National Aeronautics and Space Administration. PHYSICAL SIGNIFICANCE OF THE TIROS II RADIATION EXPERIMENT. R. A. Hanel, GSFC, and D. Q. Wark, U.S. Weather Bureau. (Presented at Optical Society of America Meeting, Pittsburgh, Pennsylvania, March 1961.) December 1961. 16p. OTS price, \$0.50. (NASA TECHNICAL NOTE D-701)</p> <p>The meteorological satellite Tiros II carries a five-channel radiometer which scans the earth as the satellite rotates. Two channels are sensitive to sunlight reflected from the earth; three are responsive to terrestrial infrared emission. The effect of the optical properties upon the measurements is discussed. Calculations, based on model atmospheres, show the sources of outgoing terrestrial radiation and limb-darkening effects for two of the channels. A map of the radiation received by the channel sensitive in the window region (8 to 12μ) is compared with a conventional weather chart.</p> <p>Copies obtainable from NASA, Washington</p>	<p>I. Hanel, Rudolf A. II. Wark, D. Q. III. NASA TN D-701 IV. Weather Bureau</p> <p>(Initial NASA distribution: 17, Communications and sensing equipment, flight; 19, Electronics; 21, Geophysics and geodesy; 30, Physics, atomic and molecular; 47, Satellites.)</p>	<p>NASA TN D-701 National Aeronautics and Space Administration. PHYSICAL SIGNIFICANCE OF THE TIROS II RADIATION EXPERIMENT. R. A. Hanel, GSFC, and D. Q. Wark, U.S. Weather Bureau. (Presented at Optical Society of America Meeting, Pittsburgh, Pennsylvania, March 1961.) December 1961. 16p. OTS price, \$0.50. (NASA TECHNICAL NOTE D-701)</p> <p>The meteorological satellite Tiros II carries a five-channel radiometer which scans the earth as the satellite rotates. Two channels are sensitive to sunlight reflected from the earth; three are responsive to terrestrial infrared emission. The effect of the optical properties upon the measurements is discussed. Calculations, based on model atmospheres, show the sources of outgoing terrestrial radiation and limb-darkening effects for two of the channels. A map of the radiation received by the channel sensitive in the window region (8 to 12μ) is compared with a conventional weather chart.</p> <p>Copies obtainable from NASA, Washington</p>	<p>I. Hanel, Rudolf A. II. Wark, D. Q. III. NASA TN D-701 IV. Weather Bureau</p> <p>(Initial NASA distribution: 17, Communications and sensing equipment, flight; 19, Electronics; 21, Geophysics and geodesy; 30, Physics, atomic and molecular; 47, Satellites.)</p>	<p>NASA</p>
<p>NASA TN D-701 National Aeronautics and Space Administration. PHYSICAL SIGNIFICANCE OF THE TIROS II RADIATION EXPERIMENT. R. A. Hanel, GSFC, and D. Q. Wark, U.S. Weather Bureau. (Presented at Optical Society of America Meeting, Pittsburgh, Pennsylvania, March 1961.) December 1961. 16p. OTS price, \$0.50. (NASA TECHNICAL NOTE D-701)</p> <p>The meteorological satellite Tiros II carries a five-channel radiometer which scans the earth as the satellite rotates. Two channels are sensitive to sunlight reflected from the earth; three are responsive to terrestrial infrared emission. The effect of the optical properties upon the measurements is discussed. Calculations, based on model atmospheres, show the sources of outgoing terrestrial radiation and limb-darkening effects for two of the channels. A map of the radiation received by the channel sensitive in the window region (8 to 12μ) is compared with a conventional weather chart.</p> <p>Copies obtainable from NASA, Washington</p>	<p>I. Hanel, Rudolf A. II. Wark, D. Q. III. NASA TN D-701 IV. Weather Bureau</p> <p>(Initial NASA distribution: 17, Communications and sensing equipment, flight; 19, Electronics; 21, Geophysics and geodesy; 30, Physics, atomic and molecular; 47, Satellites.)</p>	<p>NASA TN D-701 National Aeronautics and Space Administration. PHYSICAL SIGNIFICANCE OF THE TIROS II RADIATION EXPERIMENT. R. A. Hanel, GSFC, and D. Q. Wark, U.S. Weather Bureau. (Presented at Optical Society of America Meeting, Pittsburgh, Pennsylvania, March 1961.) December 1961. 16p. OTS price, \$0.50. (NASA TECHNICAL NOTE D-701)</p> <p>The meteorological satellite Tiros II carries a five-channel radiometer which scans the earth as the satellite rotates. Two channels are sensitive to sunlight reflected from the earth; three are responsive to terrestrial infrared emission. The effect of the optical properties upon the measurements is discussed. Calculations, based on model atmospheres, show the sources of outgoing terrestrial radiation and limb-darkening effects for two of the channels. A map of the radiation received by the channel sensitive in the window region (8 to 12μ) is compared with a conventional weather chart.</p> <p>Copies obtainable from NASA, Washington</p>	<p>I. Hanel, Rudolf A. II. Wark, D. Q. III. NASA TN D-701 IV. Weather Bureau</p> <p>(Initial NASA distribution: 17, Communications and sensing equipment, flight; 19, Electronics; 21, Geophysics and geodesy; 30, Physics, atomic and molecular; 47, Satellites.)</p>	<p>NASA</p>